Applied Mathematical Modelling 37 (2013) 4874–4882

Contents lists available at SciVerse ScienceDirect

Applied Mathematical Modelling

journal homepage: www.elsevier.com/locate/apm

# Macromodeling of high-speed interconnects by positive interpolation of vertical segments ☆

Oliver Salazar Celis [a], Annie Cuyt [a,*], Dirk Deschrijver [b], Dries Vande Ginste [b], Tom Dhaene [b], Luc Knockaert [b]

[a] Department of Mathematics and Computer Science, University of Antwerp, Middelheimlaan 1, 2020 Antwerpen, Belgium
[b] Department of Information Technology, Ghent University, Sint-Pietersnieuwstraat 41, 9000 Gent, Belgium

ARTICLE INFO

*Article history:*
Received 13 February 2012
Received in revised form 24 August 2012
Accepted 25 September 2012
Available online 13 October 2012

*Keywords:*
Macromodel
Rational model
Transmission line
On-chip interconnect
Signal integrity

ABSTRACT

In this paper a novel macromodeling scheme is presented to model the per unit of length (p.u.l.) parameters of uniform transmission lines. In particular, it is focused on single on-chip interconnects, because their p.u.l. parameters are influenced by the presence of semiconductor (s) and as such exhibit a strong frequency-dependency, making the modeling process harder. Starting from a set of very accurate tabulated data samples, obtained by two-dimensional electromagnetic modeling, rational models for the four p.u.l. parameters are constructed. The novelty of the approach lies in the fact that the rational models are positive by construction and that a controllable accuracy is obtained. These models can then further be used to construct multivariate models, e.g., for variability analysis. Here, the novel scheme is applied to an on-chip inverted embedded microstrip line, of which the signal integrity behavior is assessed in both the frequency and the time domain, demonstrating the applicability of the macromodels.



## 1. Introduction

State-of-the-art interconnect design is very challenging. Designers are facing ever more stringent design specifications — expressed in terms of bandwidth, speed, crosstalk, signal attenuation, etc. — that dictate the need for powerful modeling tools. It is of a paramount importance that these tools are able to very accurately incorporate all substrate loss mechanisms and the finite conductivity and shape of the metallic interconnects. From this perspective, macromodels describing all high-frequency behavior are extremely useful to analyze the signal integrity (SI) behavior of the interconnects.

Often, interconnect structures are characterized by using their cross-sectional geometry in a two-dimensional (2-D) electromagnetic (EM) simulation, leading up to a corresponding transmission line model [1]. An accurate description of the interconnects is then provided in terms of their per unit of length (p.u.l.) resistance ($R$), inductance ($L$), conductance ($G$) and capacitance ($C$) parameters, yielding so-called $RLGC(f)$ models. Here, $f$ denotes the frequency, as such indicating the frequency-dependent character of the p.u.l. parameters. For a comprehensive overview of such modeling methods, the reader is encouraged to consult [1] and the references therein. For on-chip lines that are electrically very short, sometimes, the p.u.l. resistance $R$ and capacitance $C$ are dominant ($RC$ regime). In the present paper, however, all four p.u.l. parameters are considered, making the approach more general and also valid at very high frequencies. Thereto, a very accurate 2-D EM modeling procedure, making use of a Dirichlet-to-Neumann (DtN) boundary operator, is used as a starting point [2]. This method

☆ This work is supported by the Research Foundation flanders (FWO-Vlaanderen). Dirk Deschrijver is a post-doctoral research fellow of FWO-Vlaanderen.
* Corresponding author.
*E-mail address:* annie.cuyt@ua.ac.be (A. Cuyt).

0307-904X/$ - see front matter © 2012 Elsevier Inc. All rights reserved.
http://dx.doi.org/10.1016/j.apm.2012.09.068

allows to accurately predict all adverse effects induced, e.g., by the finite conductivity of the metallic interconnects (skin effect) and by the semiconductors (slow-wave effects [3]. However, the modeling tool described in [2] as such is not sufficient to be useful for state-of-the-art interconnect design, because, although accurate, this EM modeling technique on its own is rather slow and only yields tabulated p.u.l. data.

In [4] it was proposed to apply the vector fitting (VF) technique [5–7] to the complex p.u.l. impedance $Z = R + j\omega L$ and to the complex p.u.l. admittance $Y = G + j\omega C$ (where $\omega = 2\pi f$ is the angular frequency) of an on-chip transmission line, yielding broadband rational macromodels. The rational macromodels, so obtained, constitute essential building blocks to compute multivariate macromodels for stochastic model-based variability analysis [8,9] or can be immediately used for SI analysis. A limitation of this complex fitting approach [4] is, however, that it leads to modeling errors that are potentially unbalanced between the different $RLGC(f)$ parameters. Also, it is essential that all four p.u.l. parameters are strictly positive [10]. Using the technique described in [4], this requirement can only be assessed and possibly enforced a posteriori when needed.

In the present paper, a different approach is proposed to develop broadband macromodels with p.u.l. parameters that are positive by construction, and this with a controllable accuracy. Rather than fitting the complex p.u.l. impedance and admittance of the line, guaranteed positive models are computed for the four real-valued $RLGC(f)$ parameters individually. To this end, a reliable technique for positive rational interpolation of the p.u.l. parameters is proposed. In particular, by performing the interpolation over well-defined data intervals, it is possible to specify explicit frequency-dependent accuracy constraints on each individual p.u.l. parameter. The technique is applied to a realistic application example, i.e. an on-chip inverted embedded microstrip (IEM) line, which was especially selected because it exhibits all potential substrate and conductor loss mechanisms.

In Section 2, the application example, i.e. the IEM line, is introduced and it is briefly explained how its tabulated $RLGC(f)$ responses are obtained using the 2-D EM tool. Next, in Section 3, the novel rational interpolation technique is thoroughly explained. In Section 4, first, the rational macromodeling technique is applied to the p.u.l. parameters of the IEM line, demonstrating the controllable accuracy. Next, the macromodels are deployed to assess the SI behavior of a source-line-load configuration, both in frequency and in time domain. Conclusions are summarized in Section 5.

## 2. Application example

### 2.1. Geometry

In this paper, as a case study, we choose an on-chip interconnect structure, i.e. the on-chip IEM line presented in Fig. 1 is considered. The build-up comprises a 30 μm thick doped silicon substrate with a relative permittivity $\epsilon_r = 11.7$ and conductivity $\sigma = 10$ S/m. On top of the silicon semiconductor, an 11.4 μm thick $SiO_2$ insulator with a relative permittivity $\epsilon_r = 3.9$ and loss tangent $\tan\delta = 0.001$ is present. The line consists of a metallic strip with a width of 2 μm and a height of 2 μm that is embedded in the $SiO_2$, 6.4 μm above the semiconductor–insulator interface. A 3 μm thick plate on top of the insulator serves as the ground plane of the microstrip line. Both the line and the ground plate are Aluminum, with a conductivity of $3.77 \cdot 10^7$ S/m.

We opt for this particular on-chip interconnect example because it exhibits dispersive and slow-wave effects [3]. Hence, the p.u.l. parameters are strongly frequency-dependent (see also Section 4.1), obviously making the modeling process hard-

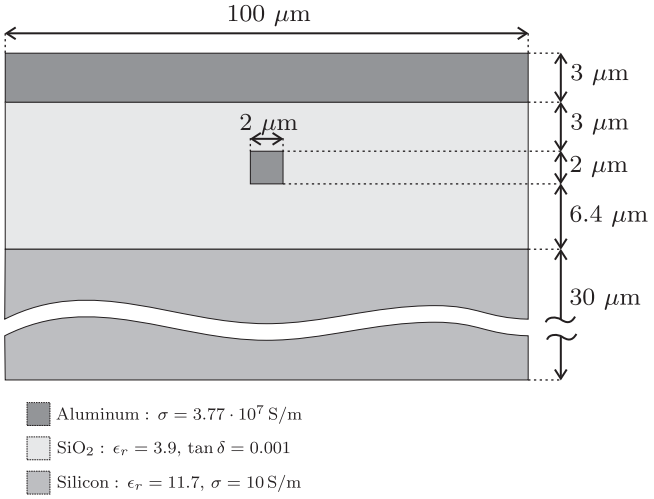


**Fig. 1.** Material properties and geometrical details of the on-chip IEM line under investigation (not on scale).

er. It is also interesting to mention that the specific topology of Fig. 1, with a top-plate ground, is gaining importance in high-frequency IC-design [11], making it an important case study anyhow.

### 2.2. Accurate tabulated RLGC($f$) computation

The procedure described in [2] allows to accurately compute the p.u.l. transmission line parameters of the structure presented in Fig. 1, by adopting a quasi-TM behavior of the fields and a careful definition of the circuit currents in the presence of the semiconductor. This leads to a consistent formulation of the complex inductance and complex capacitance problem, which are cast as boundary integral equations (BIEs). This is made possible thanks to a (discretized) differential surface admittance operator (i.e. a Dirichlet-to-Neumann operator). The BIEs are solved at a discrete number of frequencies, yielding the *tabulated* p.u.l. *RLGC*($f$) parameters. With this procedure, costly volume discretization is avoided, while still maintaining excellent accuracy, encompassing skin effect and slow-wave phenomena.

## 3. Positive rational approximation

This section describes a novel approach to develop broadband macromodels that are positive by construction, starting from the tabulated *RLGC*($f$) data of Section 2.2. Rather than fitting the complex p.u.l. admittance and impedance of the line, a guaranteed positive interpolation scheme is presented to model the four real-valued *RLGC*($f$) parameters individually. The macromodel for an arbitrary p.u.l. parameter $X$ (where $X$ stands for $R, L, G$, and $C$) are constructed from frequency-dependent data samples $X_i = X(f_i)$.

### 3.1. Barycentric interpolation formula

Given $n+1$ tabulated data $(f_i, X_i) \in \mathbb{R}^2$, the barycentric interpolation formula [12–18] can be applied to obtain a rational function expression

$$r_n(f) = \frac{\sum_{i=0}^{n} X_i \frac{u_i}{f-f_i}}{\sum_{i=0}^{n} \frac{u_i}{f-f_i}}, \quad u_i \neq 0 \tag{1}$$

that interpolates the values $X_i$ at the $f_i$ for any non-zero weights $u_i$, hence $r_n(f_i) = X_i$. A key advantage of the barycentric formula (1) is that the flexible choice of weights $u_i$ makes it possible to impose certain shape preserving properties as reported in [19]. In the current paper, some of the ideas in [19] are picked up, and a novel procedure is proposed to determine weights $u_i$ such that the resulting rational function $r_n(f)$ is guaranteed to be pole-free and positive over the entire frequency axis $[0, +\infty[$. It is obvious that $X_i > 0$ is mandatory for positivity of $r_n(f)$, a requirement that is fulfilled by using the accurate 2-D EM solver of Section 2.2 to construct the tabulated samples.

### 3.2. Pole-free over the frequency axis

Let the frequency samples $f_i$ be ordered in such a way that $a < f_0 < f_1 < \cdots < f_n < b$. Note that strict inequality at the endpoints in merely a technical assumption which is needed further on in Eqs. 3 and 4. For an irreducible rational function $r_n(f)$ to be free of poles on the entire frequency axis, it is known [12] that the $u_i$ in (1) must alternate in sign with

$$u_i u_{i+1} < 0, \quad i = 0, \ldots n-1.$$

Since the values of the $u_i$ are only defined up to a constant multiple, i.e. a normalization of $r_n(f)$, it is natural to define $u_i = (-1)^i \hat{u}_i$ or $u_i = (-1)^{i+1} \hat{u}_i$ and simply look for values $\hat{u}_i$ with a fixed sign instead. Here we take $\hat{u}_i > 0$ and explain below which sign for $u_i$ is ultimately chosen.

### 3.3. Guaranteed positivity constraints

For guaranteed positivity, additional constraints for the weights are imposed. Denote by

$$\ell(f) = \prod_{k=0}^{n} (f - f_k), \quad \ell_i(f) = \prod_{k=0, k\neq i}^{n} (f - f_k).$$

After multiplying both the numerator and denominator in the representation (1) of $r_n(f)$ with $\ell(f)$, it is easily seen that the numerator and denominator polynomials of $r_n(f) = p_n(f)/q_n(f)$ are respectively

$$p_n(f) = \sum_{i=0}^{n} X_i u_i \ell_i(f), \quad q_n(f) = \sum_{i=0}^{n} u_i \ell_i(f).$$

In order to obtain a rational function $r_n(f)$ that is positive on an interval $[a, b]$, the sign of $p_n(f)$ and $q_n(f)$ on $[a, b]$ should be the same. Without loss of generality, we aim for $q_n(f) > 0$.

A necessary condition for $q_n(f)$ to be positive on $[a,b]$ is obviously $q_n(f_i) > 0$ for all $i = 0,\ldots,n$. With the presumed ordering of the points $f_i$, the values $\ell_i(f_i)$ alternate in sign and $\ell_n(f_n) > 0$. Because $q_n(f_i) = u_i\ell_i(f_i)$, it is clear that $u_n > 0$is also required, and therefore the following convention is adopted

$$u_i = (-1)^{n-i}\hat{u}_i, \quad \hat{u}_i > 0, \quad i = 0,\ldots,n. \tag{2}$$

It is shown in [19] that a sufficient condition for the denominator polynomial $q_n(f)$ not to change sign in $[a,b]$ is,

$$\begin{aligned} &\frac{\hat{u}_{i-1}}{b-f_{i-1}} - \frac{\hat{u}_i}{b-f_i} < 0, \quad i = 1,\ldots,n, \\ &-\frac{\hat{u}_i}{f_i-a} + \frac{\hat{u}_{i+1}}{f_{i+1}-a} < 0, \quad i = 0,\ldots,n-1. \end{aligned} \tag{3}$$

Taking into account that all $X_i$ have the same sign, a sufficient condition for the numerator polynomial $p_n(f)$ not to change sign in $[a,b]$ is obtained in an analogous way

$$\begin{aligned} &X_{i-1}\frac{\hat{u}_{i-1}}{b-f_{i-1}} - X_i\frac{\hat{u}_i}{b-f_i} < 0, \quad i = 1,\ldots,n, \\ &-X_i\frac{\hat{u}_i}{f_i-a} + X_{i+1}\frac{\hat{u}_{i+1}}{f_{i+1}-a} < 0, \quad i = 0,\ldots,n-1. \end{aligned} \tag{4}$$

Hence, for given $X_i$ (either all positive or all negative), the combined linear inequalities in (2), (3) and (4) allow to find weights $\hat{u}_i$ (or $u_i$), such that the sign of the corresponding interpolating rational function $r_n(f)$ agrees with that of the $X_i$ on the entire interval $[a,b]$. Positivity over the entire frequency axis can be ensured by conformally mapping the half open interval $[0,+\infty[$ to the closed interval $[a,b] = [-1,1]$ using a standard Möbius transformation.

### 3.4. Interval interpolation

To obtain a low (er) model complexity while maintaining a desired accuracy, the point values $X_i$ are relaxed to *intervals* $\mathcal{X}_i = [\underline{X}_i, \overline{X}_i]$ and the concept of *interval interpolation* [19] is used. Hence, rather than a point value $X_i$, an interval $\mathcal{X}_i = [\underline{X}_i, \overline{X}_i]$ is given at each frequency $f_i$. Typically, the bounds $\underline{X}_i < \overline{X}_i$ are user-specified thresholds indicating the maximum allowed deviation from $X_i$.

The problem statement then becomes the following. Given $N+1$ points $f_i$ and intervals $\mathcal{X}_i$, take any $n+1$ points $f_{i_j}$ among them with $n < N$ and search for $n+1$ values $Y_{i_j} \in \mathcal{X}_{i_j}$ as well as nonzero weights $u_j$, $j = 0,\ldots,n$, such that the rational function

$$R_n(f) = \frac{\sum_{j=0}^{n} Y_{i_j}\frac{u_j}{f-f_{i_j}}}{\sum_{j=0}^{n}\frac{u_j}{f-f_{i_j}}}, \quad u_j \neq 0 \tag{5}$$

satisfies the interpolation conditions

$$R_n(f_i) \in \mathcal{X}_i, \quad i = 0,\ldots,N. \tag{6}$$

A graphical illustration hereof is shown in Fig. 2. Essentially, this formulation allows *explicit error control* for each individual p.u.l. parameter.

In [19] straightforward quadratic conditions in $u_i$ and $Y_{i_j}$ are given such that the interpolation conditions (6) are satisfied. Next we show how these interpolation conditions can be satisfied from merely linear conditions. The key to the novel linear conditions is to introduce the new variable $v_j = Y_{i_j}u_j$ and write $R_n(f)$ as

$$R_n(f) = \frac{\sum_{j=0}^{n}\frac{v_j}{f-f_{i_j}}}{\sum_{j=0}^{n}\frac{u_j}{f-f_{i_j}}}, \quad u_j \neq 0. \tag{7}$$

Assuming that $u_j$ is given as in (2), let

$$v_j = (-1)^{n-j}Y_{i_j}\hat{u}_j = (-1)^{n-j}\hat{v}_j. \tag{8}$$

Since we imposed that $\hat{u}_j > 0$, the sign of $\hat{v}_j$ depends only on the sign of $Y_{i_j}$.

The interpolation conditions $R_n(f_{i_j}) = Y_{i_j} \in \mathcal{X}_{i_j}$ at the points $f_{i_j}$ can thus be written as

$$\begin{aligned} &\underline{X}_{i_j} \leqslant \frac{\hat{v}_j}{\hat{u}_j} \leqslant \overline{X}_{i_j} \\ \iff &\begin{cases} -\hat{v}_j + \hat{u}_j\underline{X}_{i_j} & \leqslant 0 \\ \hat{v}_j - \hat{u}_j\overline{X}_{i_j} & \leqslant 0 \end{cases}, \quad j = 0,\ldots,n. \end{aligned} \tag{9}$$

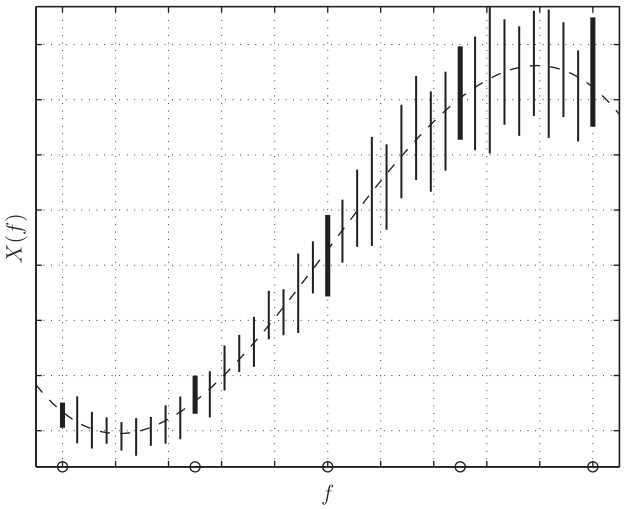


**Fig. 2.** Graphical illustration of interval interpolation. Each vertical segment is an interval $[\underline{X}_i, \overline{X}_i]$ at frequency $f_i (i = 0, \ldots, N)$. The circles ($\circ$) indicate chosen frequencies $f_{i_j} (j = 0, \ldots, n)$ for the representation (5). The dashed curve represents a rational function $R_n(f)$ satisfying (6). It intersects each interval $\mathcal{X}_{i_j}$ (shown as thick segment) at a value $Y_{i_j}$ and all other intervals (shown as regular segments) at further unspecified values.

Before considering the remaining interpolation conditions, denote the numerator and denominator polynomials of $R_n(f)$ as before by

$$P_n(f) = \sum_{j=0}^{n} v_j \ell_{i_j}(f), \quad Q_n(f) = \sum_{j=0}^{n} u_j \ell_{i_j}(f),$$

where

$$\ell_{i_j}(f) = \prod_{k=0, k\neq j}^{n} (f - f_{i_k}).$$

Given that $Q_n(f_i) > 0$, a condition previously ensured, the interval interpolation conditions $R_n(f_i) \in \mathcal{X}_i$ for $i \neq i_j$ are

$$\underline{X}_i \leqslant \frac{P_n(f_i)}{Q_n(f_i)} \leqslant \overline{X}_i$$

$$\iff \begin{cases} -P_n(f_i) + \underline{X}_i Q_n(f_i) & \leqslant 0 \\ P_n(f_i) - \overline{X}_i Q_n(f_i) & \leqslant 0 \end{cases}. \tag{10}$$

Note that these conditions are linear inequalities in the unknowns $\hat{v}_j$ and $\hat{u}_j$. Once $v_j$ and $u_j$ are determined, $Y_{i_j}$ can also be determined and $R_n(f)$ can again be written in the barycentric form if desired, e.g. for its evaluation. As pointed out in [19], it is not crucial which points $f_{i_j}$ from $\{f_0, \ldots, f_n\}$ are chosen to construct $R_n(f)$. Only the value of $n$ matters. If for a certain fixed $n$ there exists an $R_n(f)$ satisfying (6), then such an $R_n$ can be established for any choice of (distinct) $f_{i_j}$.

### 3.5. Optimization routine

After fixing the value $n$ and choosing points $f_{i_j}$ $(j = 0, \ldots, n)$ among the given $f_i$ for the representation (7), coefficients $\hat{v}_j, \hat{u}_j > 0$ satisfying the homogeneous linear inequalities (3), (4), (9) and (10) need to be found. This issue is discussed next.

Denote the vector of unknown coefficients by

$$\mathbf{c} = (\hat{v}_0, \ldots, \hat{v}_n, \hat{u}_0, \ldots, \hat{u}_n)^T \in \mathbb{R}^{2n+2}$$

and denote by $\mathbf{A}$ the $(2N + 6n + 4) \times (2n + 2)$ constraint matrix constructed from the linear inequalities (3) for $\hat{u}_j$, (4) for $\hat{v}_j = Y_{i_j}\hat{u}_j$, (9) and (10), and the strict positive conditions $\hat{u}_j > 0$ and $\hat{v}_j > 0$ which need to be established. In order to obtain a maximally robust and nontrivial vector $\mathbf{c} \neq \mathbf{0}$ in the interior of the corresponding unbounded polyhedral cone [20]

$$\{\mathbf{c} \in \mathbb{R}^{2n+2} | \mathbf{A}\mathbf{c} \leqslant \mathbf{0}\}, \tag{11}$$

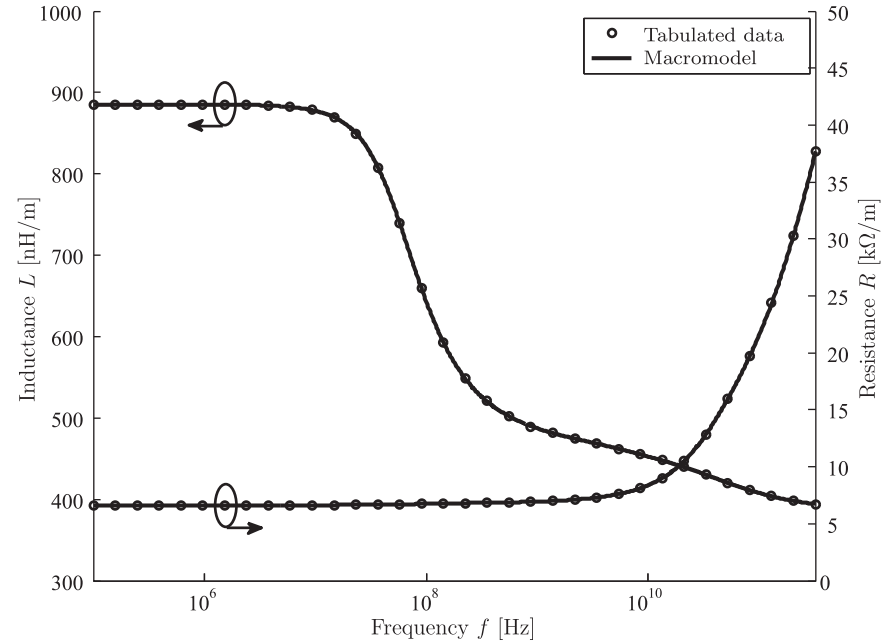


(a) Inductance $L$ and resistance $R$

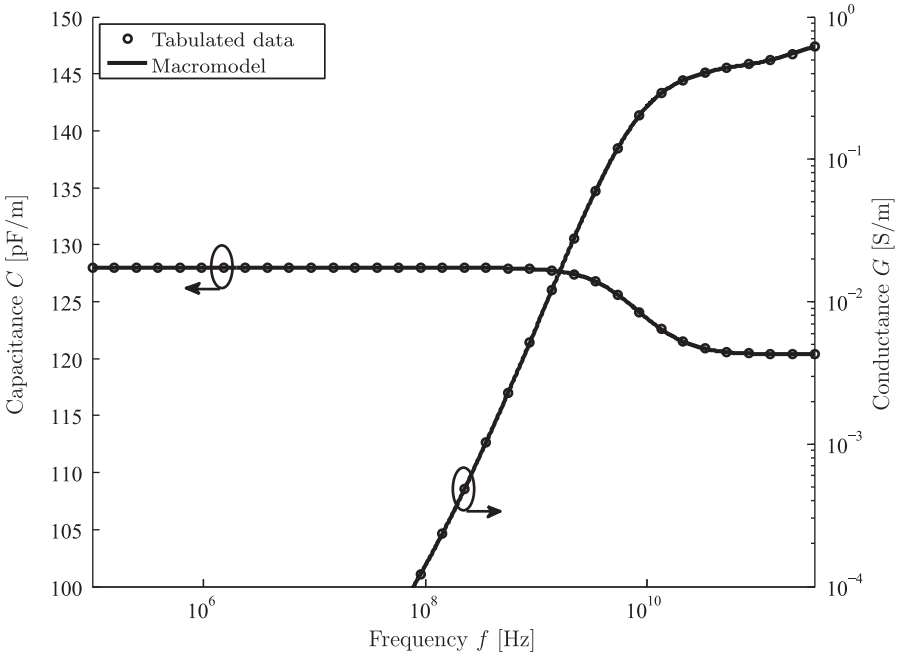


(b) Capacitance $C$ and conductance $G$

**Fig. 3.** Macromodels (full line) and tabulated samples (markers ∘) of the four p.u.l. parameters of the IEM line of Fig. 1. For clarity, only one third of the tabulated data samples are shown.

we propose the solution of the strictly convex quadratic programming (QP) problem [21]:

$$\arg \min_{\mathbf{c}\in\mathbb{R}^{2n+2}} (\|\mathbf{c}\|_2)^2$$
$$\text{subject to} \quad \mathbf{A}_j\mathbf{c} \leqslant -\delta\|\mathbf{A}_j\|_2, \quad j = 1,\ldots,2N+6n+4.$$

Here $\delta > 0$ is an arbitrary robustness margin, $\mathbf{A}_j$ denotes the $j$th row of the matrix $\mathbf{A}$ and $\|\cdot\|_2$ is the Euclidean norm. The computed vector $\mathbf{c}$ then satisfies the componentwise inequalities in (11) in a strict sense. For an in-depth discussion of the geometrical interpretation and alternative formulations, we refer to the forthcoming paper [22].

When feasible, the optimization problem above has a unique solution, which can for instance be found using the `quadprog` routine in MATLAB. This routine also assesses whether or not the optimization problem is feasible. Once values for the coefficients $\hat{v}_j$ and $\hat{u}_j$ are determined, weights $u_j$ and values $Y_{i_j}$ are obtained from (2) and (8) respectively, such that a guaranteed positive rational function of the form (5) is fully determined.

## 4. Numerical results

### 4.1. Macromodeling of the p.u.l. parameters

As an application example, the proposed novel interpolation scheme is applied to compute guaranteed positive macromodels of the real-valued $RLGC(f)$ parameters of the IEM line presented in Section 2.1. First, a tabulated set of $N+1 = 100$ data points $X_i = X(f_i)$ is calculated using the 2-D EM modeling tool of Section 2.2, where the corresponding frequencies $f_i$ are logarithmically spaced, up to 320 GHz. For each of these data points $X_i$, an interval $\mathcal{X}_i = [\underline{X}_i, \overline{X}_i]$ is constructed whose upper and lower bounds are independently chosen as

$$\underline{X}_i = X_i - \varepsilon X_i; \quad \overline{X}_i = X_i + \varepsilon X_i.$$

Here, $\varepsilon$ is a user-specified accuracy threshold that defines the maximum allowed deviation between the rational macromodel and the reference data according to a relative error criterion

$$\max_i \left( \frac{|X(f_i) - R_n(f_i)|}{|X(f_i)|} \right) < \varepsilon.$$

In order to obtain a compact model with low model orders, the value $n$ of $R_n(f)$ is chosen as follows. For increasing $n = 0, 1, 2, \ldots$ a subset of $n+1$ points $f_{i_j}$ is chosen among the given $f_i$ in a structured fashion, the feasibility of the QP problem is checked and a solution is computed if it exists. Since the data has an overall smooth behavior, it is natural to choose the $f_{i_j}$ as uniformly as possible over the interpolation interval. It is found that a value of $n = 11$ is sufficient to model all the p.u.l. parameters with a relative error $\varepsilon$ of 0.1%. Fig. 3 shows the response of the macromodel, and an excellent agreement is observed with the reference data points. The controllable accuracy is demonstrated in Fig. 4, where the actual obtained relative error on the p.u.l. capacitance $C$ is shown when using three different target accuracies $\varepsilon = 5\%$, 0.1%, 0.01% during the macromodeling process.

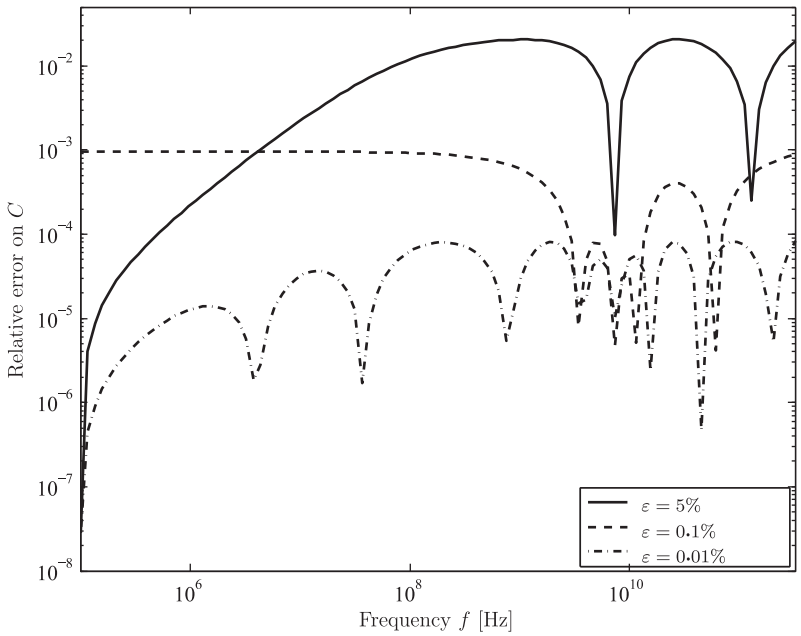


**Fig. 4.** Illustration of the controllable accuracy of the novel macromodeling scheme. The obtained relative error for the macromodel of the p.u.l. capacitance $C$ is shown when using three different target accuracies $\varepsilon$ during the modeling process.

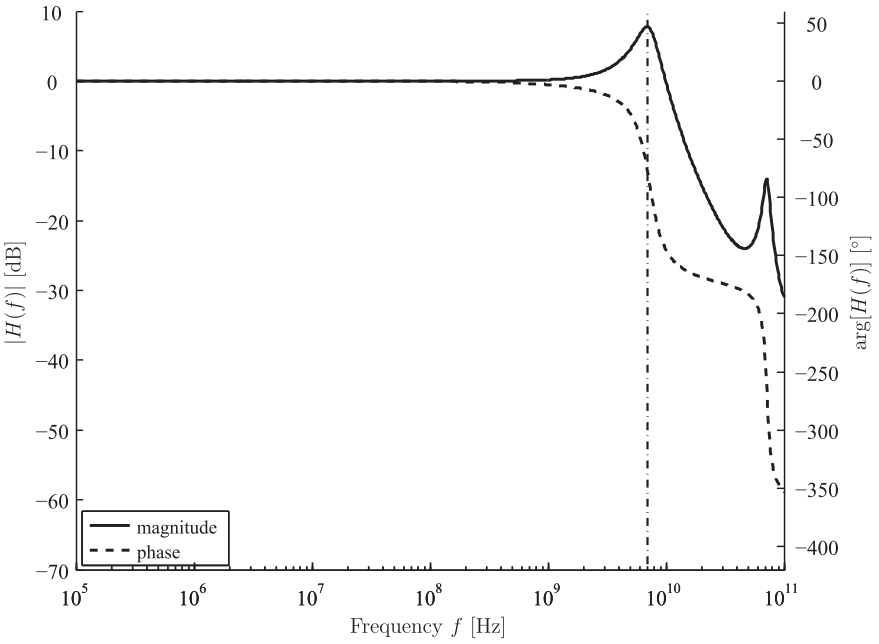


**Fig. 5.** Transfer function $H(f)$ of the source-line-load configuration.

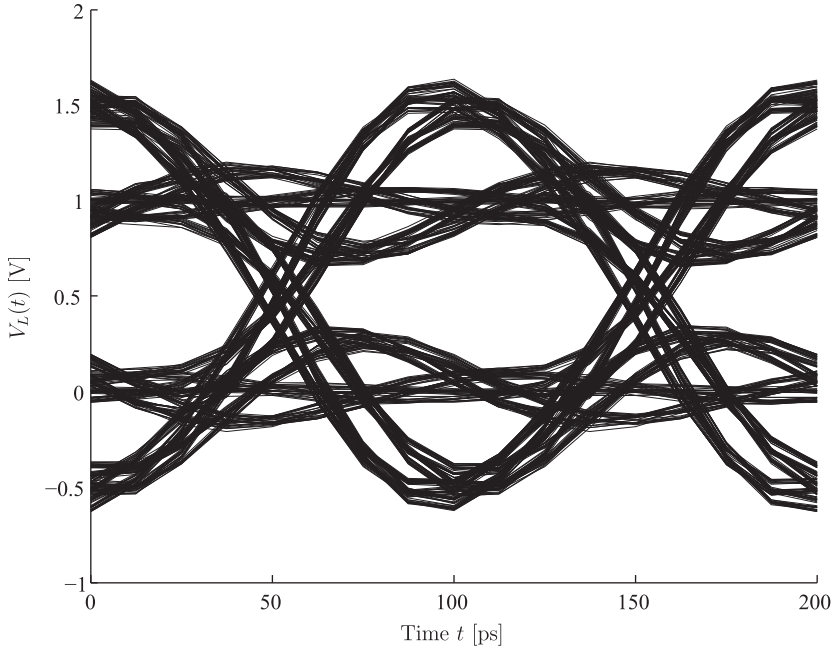


**Fig. 6.** TDT eye diagram of the source-line-load configuration.

### *4.2. Signal integrity analysis in frequency and time domain*

The applicability of the novel rational models is now demonstrated by computing relevant frequency and time domain SI characteristics. A source-line-load configuration is constructed by giving the IEM line of Fig. 1 a finite length of 1 mm. The line is driven by a low-impedance Thévenin generator composed of a voltage source $E(f)$ or $E(t)$, depending on whether we are considering frequency ($f$) or time ($t$) domain respectively, and an internal impedance of 1 Ω. The line is terminated by a capacitive load of 1 pF. In the frequency domain, we compute the transfer function $H(f) = V_L(f)/E(f)$, where $V_L(f)$ is the volt-

age at the capacitive load. The magnitude and phase of this transfer function are shown in Fig. 5. Around 7 GHz, a resonance appears. This can be attributed to the inductance of the line in combination with the capacitive load, indicating that, at high frequencies, the IEM line does no longer operate in the *RC* regime. This is further illustrated in Fig. 6 where a time domain transmissometry (TDT) eye diagram is shown. To this end, the time domain voltage source $E(t)$ produces a pseudo-random bit sequence (PRBS) with a bitrate of 10 Gbps, a rise/fall time of 50 ps and a voltage swing of 1 V. It is interesting to mention that, by generating this kind of plots starting from the rational macromodels, a design engineer can immediately assess the amount of ringing and overshoot on the line.

## 5. Conclusions

A novel macromodeling scheme for the p.u.l. parameters of transmission lines was presented. In particular, an on-chip interconnect, i.e. an IEM line, was chosen as a case study. This application example was especially selected as the presence of the semiconductor leads to p.u.l. parameters that are strongly frequency-dependent, making the macromodeling process harder. Starting from a set of accurate but tabulated $RLGC(f)$ data, four rational models are computed. The novelty of the approach lies in the fact that, by construction, the new scheme guarantees the positivity of the four models within the entire frequency range. Furthermore, it is shown that a controllable accuracy is achieved. These properties were illustrated by first applying the presented rational modeling technique to the p.u.l. parameters of the IEM line. Next, the applicability of the method was demonstrated by assessing the SI behavior of the IEM line, both in frequency and in time domain, using the novel rational models for the p.u.l. parameters.

## References

[1] F. Olyslager, Electromagnetic Waveguides and Transmission Lines, Oxford University Press Inc., New York, 1999.
[2] T. Demeester, D. De Zutter, Quasi-TM transmission line parameters of coupled lossy lines based on the Dirichlet to Neumann boundary operator, IEEE Trans. Microw. Theory Tech. 56 (7) (Jul. 2008) 1649–1660.
[3] W. Kim, M. Swaminathan, Characterization of co-planar Silicon transmission lines with and without slow-wave effect, IEEE Trans. Adv. Pack. 30 (3) (Aug. 2007) 526–532.
[4] D. Vande Ginste, D. Deschrijver, T. Demeester, T. Dhaene, D. De Zutter, "Broadband passive RLGC(f) modeling for on-chip interconnect design", in: Proceedings of the 2011 International Conference on Electromagnetics in Advanced Applications (ICEAA), Torino, Italy, Sep. 2011, pp. 1372–1375.
[5] B. Gustavsen, A. Semlyen, Rational approximation of frequency domain responses by vector fitting, IEEE Trans. Power Del. 14 (3) (Jul. 1999) 1052–1061.
[6] D. Deschrijver, M. Mrozowski, T. Dhaene, D. De Zutter, Macromodeling of multiport systems using a fast implementation of the vector fitting method, IEEE Microwave Wireless Comp. Lett. 18 (6) (Jun. 2008) 383–385.
[7] G. Antonini, D. Deschrijver, T. Dhaene, Broadband rational macromodeling based on the adaptive frequency sampling algorithm and the partial element equivalent circuit method, IEEE Trans. Electromagn. Compat. 50 (1) (Feb. 2008) 128–137.
[8] D. Deschrijver, T. Dhaene, D. De Zutter, F. Canavero, "Macromodeling based variability analysis of an inverted embedded microstrip line", in: Proceedings of the IEEE 20th Conference on Electrical Performance of Electronic Packaging and Systems (EPEPS), San Jose, CA, USA, Oct. 2011, pp. 153–156.
[9] D. Vande Ginste, D. De Zutter, D. Deschrijver, T. Dhaene, P. Manfredi, F. Canavero, Stochastic modeling based variability analysis of on-chip interconnects, IEEE Trans. Comp. Pack. Manuf. Tech. 2 (7) (Jul. 2012) 1181–1192.
[10] R. Achar, M. Nakhla, Simulation of high-speed interconnects, Proc. IEEE 89 (5) (May 2001) 693–728.
[11] W. Winkler, J. Borngraber, F. Korndorfer, C. Scheytt, "94 GHz amplifier in SiGe technology", in: Proceedings of the 38th European Microwave Conference, Amsterdam, The Netherlands, 2008, pp. 167–170.
[12] C. Schneider, W. Werner, Some new aspects of rational interpolation, Math. Comput. 47 (175) (1986) 285–299.
[13] J.P. Berrut, Rational functions for guaranteed and experimentally well-conditioned global interpolation, Comput. Math. Appl. 15 (1) (1988) 1–16.
[14] L. Knockaert, A simple and accurate algorithm for barycentric rational interpolation, IEEE Signal Process. Lett. 15 (2008) 154–157.
[15] C. Ma, Comments on a simple and accurate algorithm for barycentric rational interpolation, IEEE Signal Process. Lett. 17 (1) (2010) 111.
[16] L. Knockaert, Reply to comments on a simple and accurate algorithm for barycentric interpolation, IEEE Signal Process. Lett. 17 (1) (2010) 112.
[17] W. Werner, Polynomial interpolation: Lagrange versus Newton, Math. Comput. 43 (17) (1984) 205–217.
[18] J.P. Berrut, L.N. Trefethen, Barycentric Lagrange interpolation, SIAM Rev. 46 (3) (2004) 501–517.
[19] H.T. Nguyen, A. Cuyt, O. Salazar Celis, Comonotone and coconvex rational interpolation and approximation, Numer. Alg. 58 (2011) 1–21.
[20] S.P. Boyd, L. Vandenberghe, Convex Optimization, Cambridge University Press, 2004.
[21] O. Salazar Celis, A. Cuyt, B. Verdonk, Rational approximation of vertical segments, Numer. Alg. 45 (2007) 375–388.
[22] A. Cuyt, O. Salazar Celis, Multivariate datafitting with error control, Siam Rev., in press.